

## Article

# Microstructural and Mechanical Properties of Longitudinal Welds in Porthole Die Extrudates of a 0.5 wt.% GNP/Al Composite

Shumei Lou <sup>1</sup>, Yiming Li <sup>1</sup>, Baojia Cheng <sup>1</sup>, Lingwei Ran <sup>1</sup>, Xuefeng Bai <sup>1</sup>, Peng Chen <sup>1</sup> and Qingbiao Wang <sup>2,\*</sup>

<sup>1</sup> College of Mechanical and Electronic Engineering, Shandong University of Science and Technology, Qingdao 271019, China

<sup>2</sup> College of Resources, Shandong University of Science and Technology, Qingdao 271019, China

\* Correspondence: w18805381111@163.com; Tel.: +86-18805381111

**Abstract:** In this study, porthole die extrusion was performed on a graphene-nanoplatelet-reinforced aluminum composite (0.5 wt.% GNP/Al) prepared by powder metallurgy. The microstructure, grain size, microtexture, and mechanical properties of the composite extruded by the porthole die were studied. Along the extrusion direction, the tensile strength of the extruded composite was 139.7 MPa, and the elongation was 27.1%. Along the transverse direction, which included the weld zone, the tensile strength was 126.4 MPa, and the elongation was 24.1%. These values were 6.65% and 54.63% higher than those obtained for pure aluminum, respectively. Fractography along the extrusion direction revealed obvious ductile fracture characteristics; however, these were not so obvious along the transverse direction, mainly due to the anisotropy caused by the grain orientation of the extruded composite, thereby indicating that the composite exhibited excellent weld performance, which was further verified by Optical Microscope, Electron Backscattered Diffraction, and Transmission Electron Microscope images. Overall, these results indicate that GNP can contribute to the strength and toughness of composites in the weld zone in porthole die extrusions.

**Keywords:** porthole die; longitudinal weld; 0.5 wt.% GNP/Al composite; mechanical performance



**Citation:** Lou, S.; Li, Y.; Cheng, B.; Ran, L.; Bai, X.; Chen, P.; Wang, Q. Microstructural and Mechanical Properties of Longitudinal Welds in Porthole Die Extrudates of a 0.5 wt.% GNP/Al Composite. *Metals* **2023**, *13*, 522. <https://doi.org/10.3390/met13030522>

Academic Editor: António Bastos Pereira

Received: 3 February 2023

Revised: 28 February 2023

Accepted: 2 March 2023

Published: 5 March 2023



**Copyright:** © 2023 by the authors. Licensee MDPI, Basel, Switzerland. This article is an open access article distributed under the terms and conditions of the Creative Commons Attribution (CC BY) license (<https://creativecommons.org/licenses/by/4.0/>).

## 1. Introduction

With recent rapid developments in rail, road, and air transport, traditional aluminum alloys are often now unable to meet the manufacturing requirements of these industries. Aluminum matrix composites such as graphene-nanoplatelet-reinforced aluminum composites (GNP/Al composites) are characterized by their light weight, high strength, low thermal expansion coefficient, good thermal conductivity, low friction coefficient, good wear resistance, and other desirable properties [1–4], and they have become one of the metal matrix composites with the most potential.

Secondary deformation processes such as rolling, drawing, and extrusion are often used to improve the properties of aluminum matrix composites. The process of hot extrusion has obvious strengthening and toughening effects, and so this has become one of the principle means by which the performance of aluminum matrix composites is improved [5–8].

In recent years, researchers have carried out simple bar extrusions on aluminum matrix composites to improve the mechanical properties and microstructure of GNP/Al composites [9–13]. The hot extrusion process can improve the density of the composites, refine the grains, homogenize the microstructure, improve the dispersion, and reduce the agglomeration of the graphene nanoplatelets [14], thereby greatly enhancing the mechanical properties of the composites. However, at present, hot extrusion is performed only to obtain simple bar extrudate, in order to improve the performance of the composite. Further studies on the hot extrusion process involving GNP/Al composites to produce an aluminum-based profile with more complex sections and high strength ratio used in bearing or structural components in aerospace or rail traffic are necessary.

Porthole die extrusion is the most common method for the manufacture of aluminum-based alloy products [15–17]. During this process, the longitudinal weld zone [18] is the weakest part of the extrudate. The longitudinal weld is, therefore, of great importance when determining the overall quality of porthole die extrudates.

A number of researchers have studied the welding qualities of aluminum extrudates. Yu et al. [19] conducted a porthole die extrusion on AA6063 aluminum alloy, and studied the influence of extrusion temperature and speed on the seam welding of extrudates. They found that increasing extrusion temperature and speed not only promotes the forming of the welding interface but also closes the micro-voids at the weld, thus improving the atomic bonding on both sides of the weld and thereby promoting the hardness, tensile strength, and elongation of the extrudate. Chen et al. [20] conducted porthole die extrusions on 7075 aluminum alloy at different extrusion temperatures and found that a higher extrusion temperature leads to improvement in the solid-state welding quality of the material. Fan et al. [21] performed porthole die extrusion on 1060/6063 aluminum alloy. They obtained a good welding interface and then studied the effect of welding chamber height on the quality of solid-state welding. They found that an increase in welding chamber height can improve the welding quality. Optimal welding performance was obtained when the height of the welding chamber was 10 mm, a maximum tensile strength of 155 MPa, and a fracture strain of 0.34 were recorded. Lou et al. [15], investigated the distribution of the transverse weld of AA6061 aluminum alloy profile and studied the influence of a transverse weld on extrudate properties by considering aspects of grain size and texture type in the weld and matrix zones. Yu et al. [22] conducted a semicontinuous porthole die extrusion on homogenized 6063 aluminum alloy, and analyzed the microstructure and mechanical properties, as well as the corrosion resistance, of the longitudinal and transverse welds of the extrudate. They found that, in relative terms, the corrosion resistance and tensile properties of longitudinal welds are better than those of transverse welds.

In summary, researchers have systematically studied longitudinal and transverse welds in porthole die extrusions using aluminum alloys. However, to the best of our knowledge, there have been no studies of longitudinal welds of GNP/Al composites. In this study, 0.5 wt.% GNP/Al composites were extruded by a porthole die. The microstructure and mechanical properties of the longitudinal welds of the composites were then studied. The results obtained may provide a reference for the porthole die extrusion process, and for the solid welding of graphene-reinforced aluminum matrix composites.

## 2. Materials and Methods

### 2.1. Preparation of the Composites

High-purity spherical aluminum powder was provided by Sino-Ocean Powder Technology Co., Ltd., Xinxiang, China. This is illustrated in Figure 1a, and its main components are shown in Table 1. The average particle size was approximately 18  $\mu\text{m}$ , as shown in Figure 1b. The GNP was provided by Qingdao Huagao Graphene Technology Co., Ltd., Qingdao, China. Layers were less than 10 in number, sheet diameter was 2–4  $\mu\text{m}$ , and specific surface area was at least 230  $\text{m}^2\cdot\text{g}^{-1}$  (Table 2). Figure 1c,d show transmission electron microscopy (TEM, FEI F200X, Thermo Fisher Scientific, Waltham, MA, USA) images of the GNP which reveal its flocculent, translucent, and typical wrinkle structure characteristics. The 0.5 wt.% GNP/Al composite powders were prepared by ultrasonic dispersion and wet ball milling [23], followed by vacuum hot pressing sintering at 570  $^{\circ}\text{C}$ , to obtain hot-pressed cylindrical composite billets, as shown in Figure 2.

**Table 1.** Main components of the pure aluminum.

Element (wt.%)				
Al	Cu	Fe	Si	Water
99.95	0.0041	0.0046	0.0052	0.03

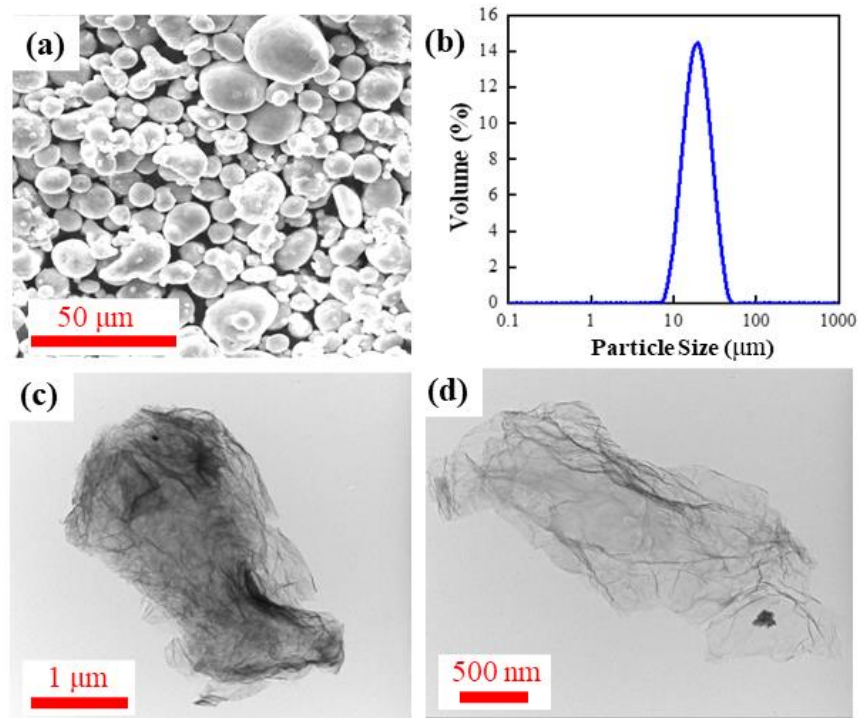


**Figure 1.** (a) SEM image of pure aluminum; (b) particle size distribution of pure aluminum; (c) TEM image of GNPs; (d) high-magnification TEM image of GNPs.

**Table 2.** Performance of the GNP.

Performance	Parameter
PH	3.5–6.0
Density (g/cm <sup>3</sup> )	<0.08
Specific surface area (m <sup>2</sup> /g)	≥230
Layers	<10
Mass fraction of carbon (%)	70 ± 5
Mass fraction of oxygen (%)	20 ± 5
Mass fraction of sulfur (%)	<0.3
Mass fraction of water (%)	<2.0

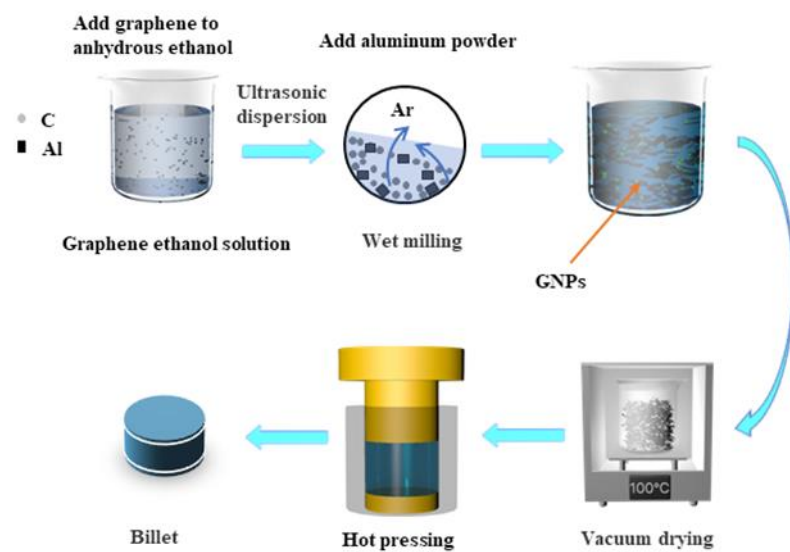


**Figure 2.** Powder metallurgy process.

## 2.2. Porthole Die Extrusion

The porthole die extrusion was performed using a 200-ton servo hydraulic press controlled by a microcomputer. The porthole die of the extrusion included a top die, a bottom die, a bridge, and a container, as shown in Figure 3. The billet was kept at 460 °C for 15 min before the extrusion, and the extrusion speed was 6 mm·min<sup>-1</sup>. Extrusion was followed by water quenching to preserve the extrusion microstructure. For comparison, the same process was carried out using pure aluminum. Figure 4 shows the load–displacement stroke curves for the composite and the pure aluminum during the porthole die extrusion and depicts the four stages of the extrusion process. At the beginning of the first upsetting stage (stage I), the upsetting of the composite with lower density due to more pores and aggregation of GNP needs a lower load compared with pure aluminum. From the latter part of the first stage and the second porthole stage (stage II), the extrusion process begins with more and more delamination and orientation of the GNP enhancing the strength of the composition which needs a larger load. While at the beginning of the welding stage (Stage III), the orientation of GNP is perpendicular to the extrusion direction, so there is a transient softening tendency on the curve for the composite. After that, the GNP with fewer layers and better dispersion enhances the performance of the aluminum matrix resulting in a larger load compared with pure aluminum.

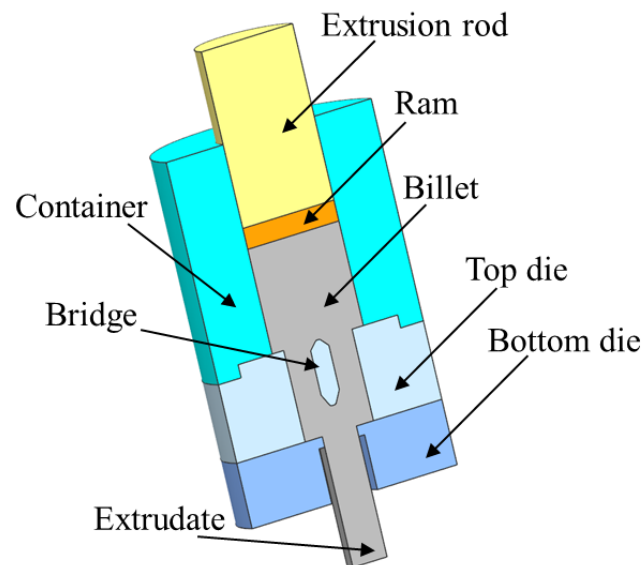


**Figure 3.** Porthole die.

## 2.3. Microstructural Characterization

An optical microscope (OM, 50X-1000X) was used to observe the microstructural morphology of the composite extrudate. To this end, a sample with dimensions of 10 × 12 × 4 mm was used, as shown in Figure 5. Keller reagent was used for the corrosion of the samples. Electron backscatter diffraction (EBSD, FEI Quanta 650F, Thermo Fisher Scientific, Waltham, MA, USA) observation of the sample was performed after ion thinning and electrolytic polishing to analyze the size, orientation, and misorientation angle of the grain, and the recrystallization of the composite. The morphology of the GNP and the interface in the welding region of the composite were characterized by field emission transmission electron microscopy (TEM, FEI Talos F200X, Thermo Fisher Scientific, Waltham, MA, USA). A field-emission scanning electron microscope (FE-SEM, model Sigma-300, Carl Zeiss AG, Germany) was used for fractography observation and for EDS elemental analysis. For hardness testing, a sample with dimensions of 15 × 15 × 8 mm was used, as shown in Figure 5, and a Raman spectrometer (LabRAM HR Evolution, Horiba, France) with a laser wavelength of 532 nm was used for detection purposes.

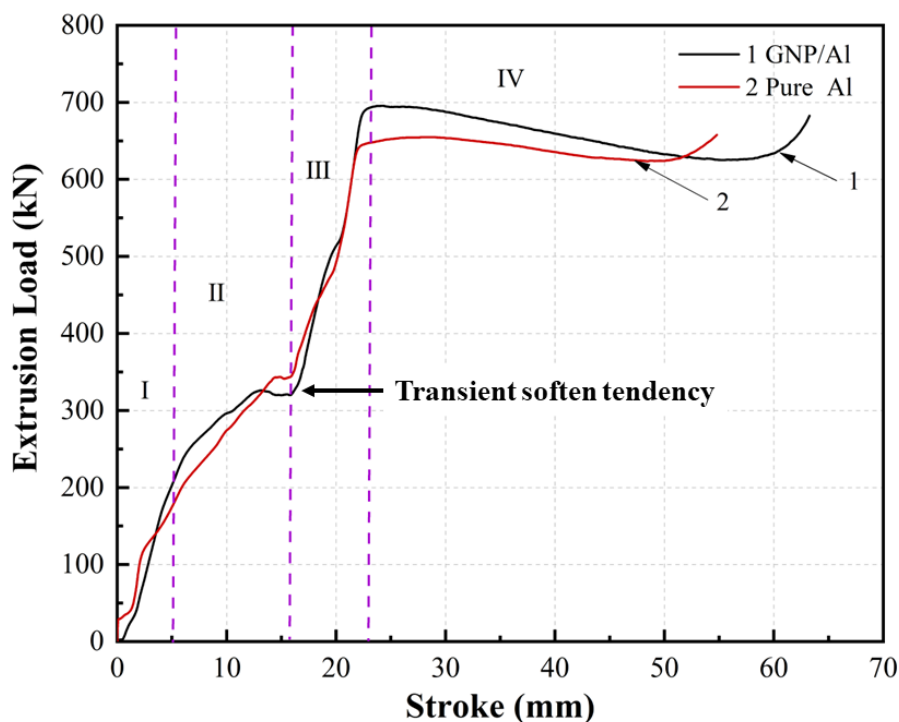


Figure 4. Load-displacement curve during the extrusion.

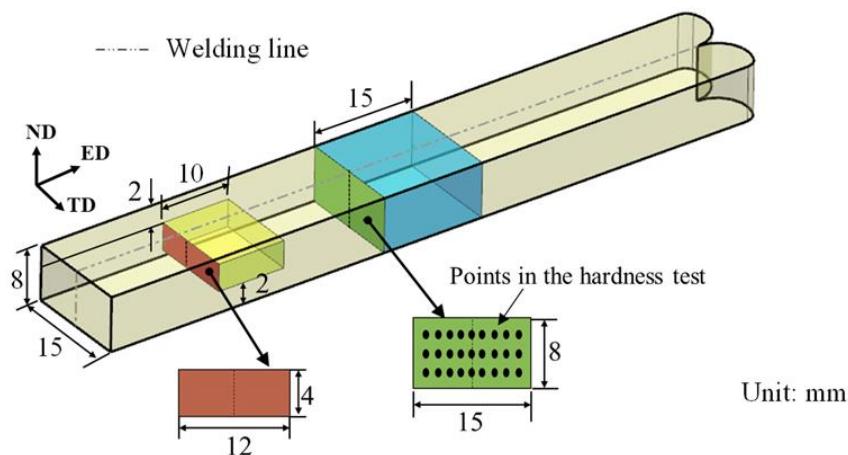
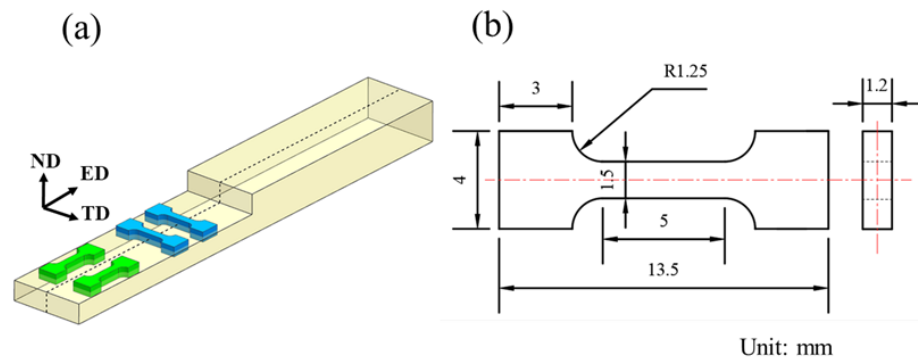


Figure 5. Schematic diagram of the samples used for characterizations.

### 2.4. Mechanical Performance

Tensile tests were carried out at room temperature using an electronic universal tensile testing machine (Zwick Z2.5 TH) with a strain rate of  $0.5 \times 10^{-3}$ /s. The locations and dimensions of the tensile samples (along the extrusion direction (ED,  $0^\circ$  direction) or along the transverse direction (TD,  $90^\circ$  direction)) were determined according to the standard of ISO 6892-1:2009, MOD, and are shown in Figure 6. Elongation and elastic modulus were measured with a laser extensometer (Zwick, USA). To test microhardness, Q10M equipment (QNESS, Austria) was used with a load of 10 g, and a holding time of 10~15 s; an average value of the three points along the ND (normal direction) was then obtained to express the hardness distribution along the lengthwise direction on the cross-section.



**Figure 6.** Sampling for tensile testing: (a) sample locations; and (b) dimensions.

### 3. Results and Discussion

#### 3.1. Microstructure

Figure 7 presents low-magnification optical images of the microstructures of cross-sections of composite and pure aluminum extrudates, and reveals differences between the weld zone and the matrix zone in both materials [24]. There are no large-sized holes at the interface of material and shunt welding, and this proves the feasibility of porthole die extrusion of GNP/Al composites. The weld zone of the composite is wider than that of pure aluminum, but its center welding zone is lighter. This indicates that the welding of the composite is better than that of pure aluminum, and this finding is consistent with the mechanical properties.

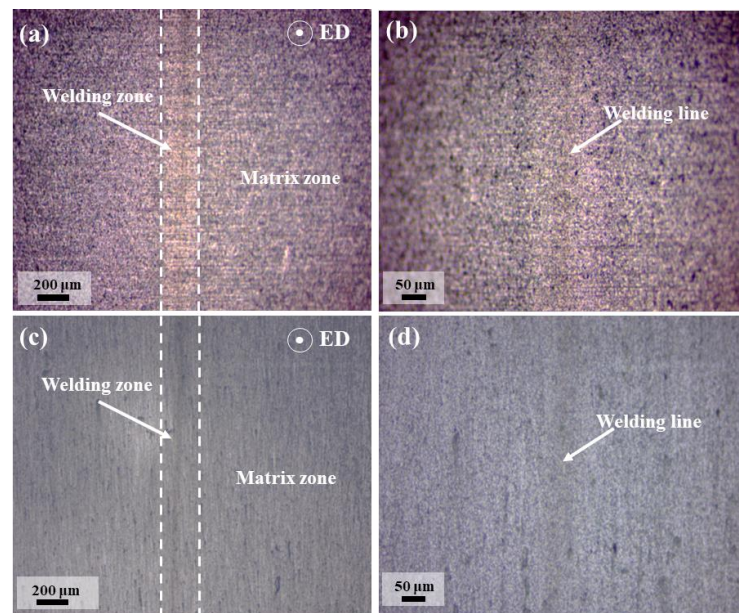


**Figure 7.** Optical microstructure near the welding zone on the cross-section of the extrudates: (a,b) composite; (c,d) pure aluminum.

#### 3.2. Raman Spectroscopy

Figure 8 shows the Raman spectra of the hot-pressed and extruded composites. The relative intensity of the D band and the G band ( $I_D/I_G$ ) indicates the degree of defectivity in the GNP layers; the relative intensity of the 2D band and the G band ( $I_{2D}/I_G$ ) reflects the layer state of the GNP [25,26]. As shown in Figure 8a, the  $I_D/I_G$  ratios of GNP/Al composites before and after the porthole die extrusion were 1.05 and 0.89, respectively. This latter value is much lower than the equivalent value for the composite extrudate obtained by solid extrusion in our previous study [27]. We may conclude, therefore, that after hot extrusion, the graphene is arranged in a directional manner. After hot extrusion, the

graphene nanosheets are flatter and are elongated along the extrusion direction. More fresh graphene is exposed by the huge shear of the extrusion process, reducing the defect density of the graphene [28]. Moreover, the large shear stress leads to better GNP delamination and better interfacial bonding between GNP and the matrix. In this study, as shown in Figure 8b, the  $I_{2D}/I_G$  ratio of the porthole-die-extruded composite was 0.30. This is a much higher value than that previously obtained for composite extrudate in solid extrusions [27], thus demonstrating the enhanced effectiveness of the GNP.

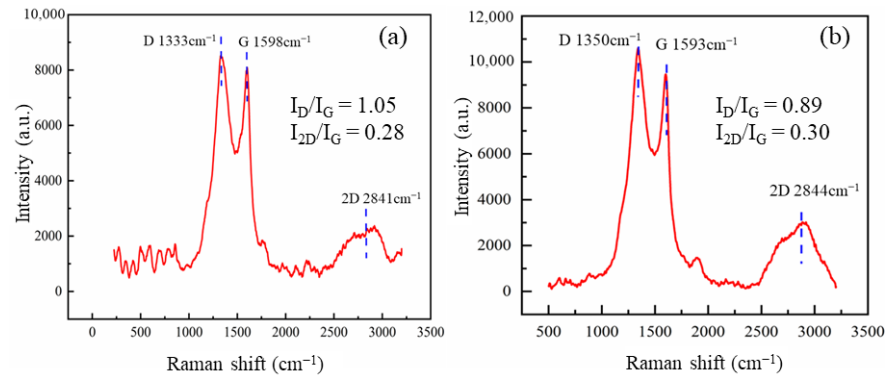


**Figure 8.** Raman spectra for (a) hot-pressed; and (b) extruded composites.

### 3.3. Grain Orientation

Figure 9 shows the EBSD mapping and the misorientation angle for the GNP/Al composite extruded by the porthole die in the welding zone and the matrix zone on a cross-section. It can be observed from the diagram that the width of the welding zone of the composite material is about 130 micrometers, and the overall bonding interface is better. Compared with the matrix zone, the grain size distribution in the welding zone is not uniform, and the proportion of small-angle grain boundaries is higher. This is consistent with the results observed by the optical microscope.

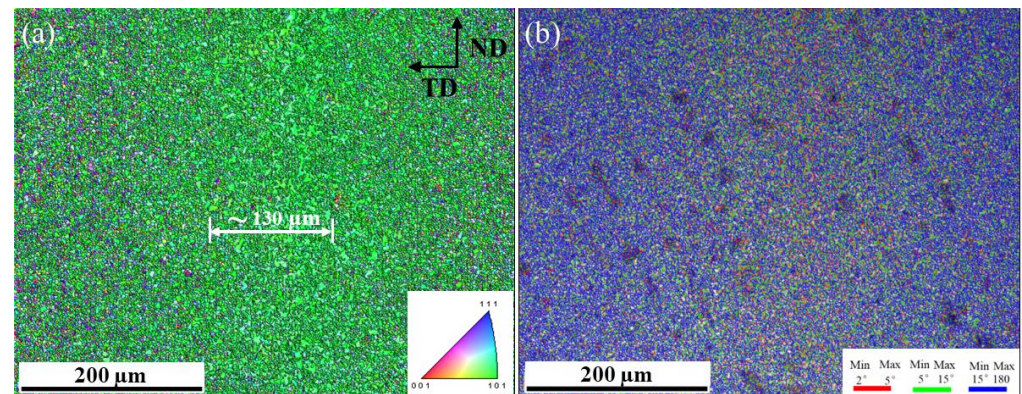


**Figure 9.** EBSD mapping and misorientation angle for the GNP/Al composite extruded by the porthole die. (The subfigure is an inverse pole graph in (a); the subfigure is misorientation angle range in (b)).

Figure 10 illustrates EBSD mapping and grain size distribution for the GNP/Al composite extruded by the porthole die along the extrusion direction in the weld and matrix zones. Grains in the matrix and weld zones are generally equiaxed [29], and many fine grains can be seen in the weld zone, indicating dynamic recrystallization. There are only a few fine grains in the matrix zone, which means that the dynamic recrystallization fraction in this zone is very small. The existence of more small grains in the weld zone is due to the fact that the aluminum here experienced a longer deformation path and more severe shear deformation, compared with the matrix zone, leading to an accumulation of higher dislocation and strain [30], and a more serious and continuous dynamic recrystallization of

the grains. However, the local temperature elevation also caused grain growth, and the formation of coarse grains, so that the uniformity of grains in the weld zone is not as high as in the matrix zone.

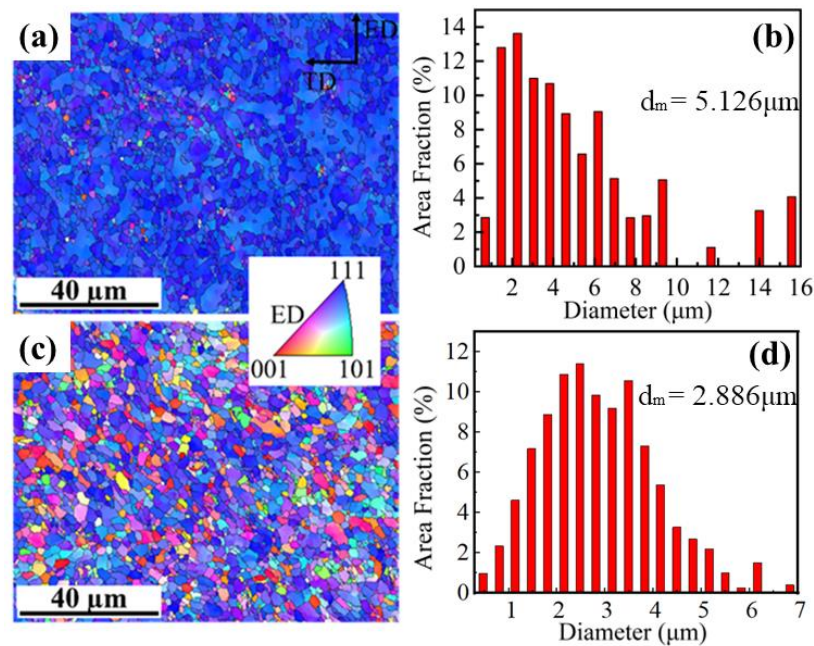


**Figure 10.** EBSD mapping and grain sizes for the GNP/Al composite extruded by the porthole die: (a,b) welding zone; (c,d) matrix zone.

Figure 11 shows the dislocation angle of the extruded composite along the extrusion direction. Owing to the high stacking-fault energy of aluminum, the proportion of subgrains formed by dynamic recovery is extremely high. Furthermore, the proportion of subgrains extruded by porthole die in this study is much higher than that obtained by solid hot extrusion [27] because of the more serious deformation and shearing of the composite. A comparison of Figure 11b,d reveals that the proportion of subgrains in the weld zone is higher than in the matrix zone, indicating that the greater the shear deformation of the material, the more the dislocation accumulation, and the greater the generation of more subgrains. This is the other reason why the proportion of high misorientation angles in the weld zone (35.91%) is lower than in the matrix zone (49.6%).

Figure 12 presents an orientation distribution function (ODF) diagram of the composite ( $\varphi_2 = 0^\circ, 45^\circ, 90^\circ$ ) extruded by the porthole die. Figure 13 shows the main textures on the ODF section and the corresponding Miller index when  $\varphi_2 = 45^\circ$  [30]. Figure 11a reveals two strong textures in the matrix zone: texture (110) [111]; and copper texture (112) [111], which is a rolling texture, as highlighted by Figure 13. Figure 12a also shows that the texture is mainly (112) [111] in the weld zone, which exhibits much higher strength than the matrix zone [21,31].

### 3.4. TEM Morphology

In order to further verify the weld quality of the GNP/Al composite, the weld zone of the composite was characterized by TEM. The results are presented in Figure 14, which shows that the grain distribution of the composite in the weld zone exhibits an obvious orientation because of the extrusion. It can also be observed that graphene is uniformly dispersed in the aluminum matrix. The low-magnification TEM images in Figure 14a–c show that the GNP with a larger size (micro level, indicated by red arrows) is mainly distributed at the grain boundary, whereas the GNP with a smaller size (nano level, indicated by yellow arrows) is distributed inside the grain, mostly along the grain orientation direction. This is because high-speed milling leads to in-plane fracturing of graphene, which greatly reduces the size of some GNP to the nanoscale, more readily during the growth of the grain [32].

The micrometer-level graphene can effectively hinder grain boundary migration, so this is likely to appear at the grain boundary and pin adjacent grains together, resulting in high fracture strain [33]. However, there is also an obvious barrier-stacking effect of graphene on dislocations at grain boundaries, as shown in Figure 14b. This effect improves the fracture strength of the composites still further. The interface of the GNP and the matrix in the weld zone of the composites was also studied by high-resolution transmission electron microscopy. From Figure 14d,e, it can be observed that graphene directly contacts the aluminum matrix, and GNP/Al composites exhibit close interface bonding [34]. In the low-magnification TEM images,  $Al_4C_3$  can also be seen occasionally [35], obliquely inserted at the boundary of the GNP and the aluminum. This plays a role in pinning the interface and improving the interfacial bonding strength, as shown in Figure 14c,f.

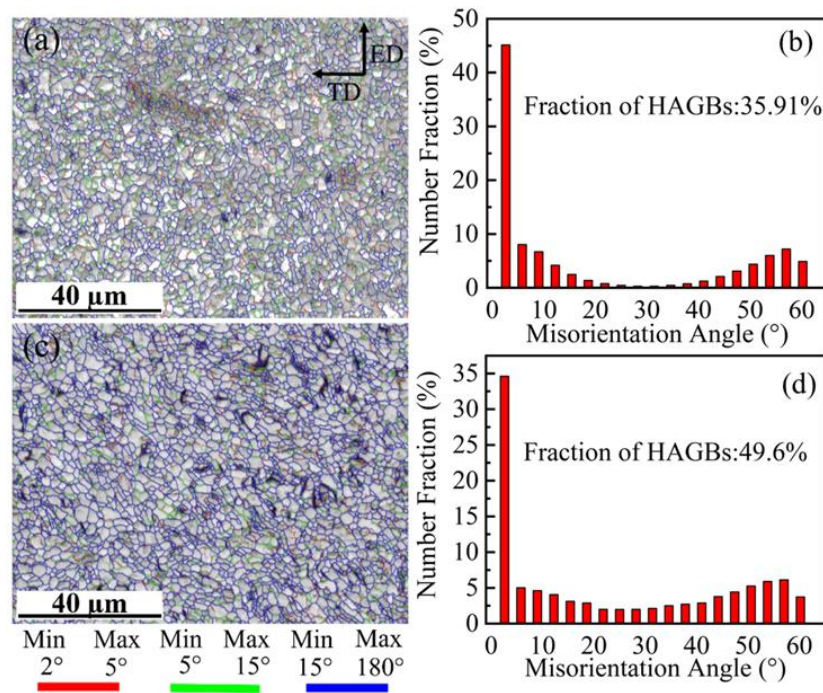


Figure 11. Misorientation angle diagram of the extruded composite: (a,b) welding zone; (c,d) matrix zone.

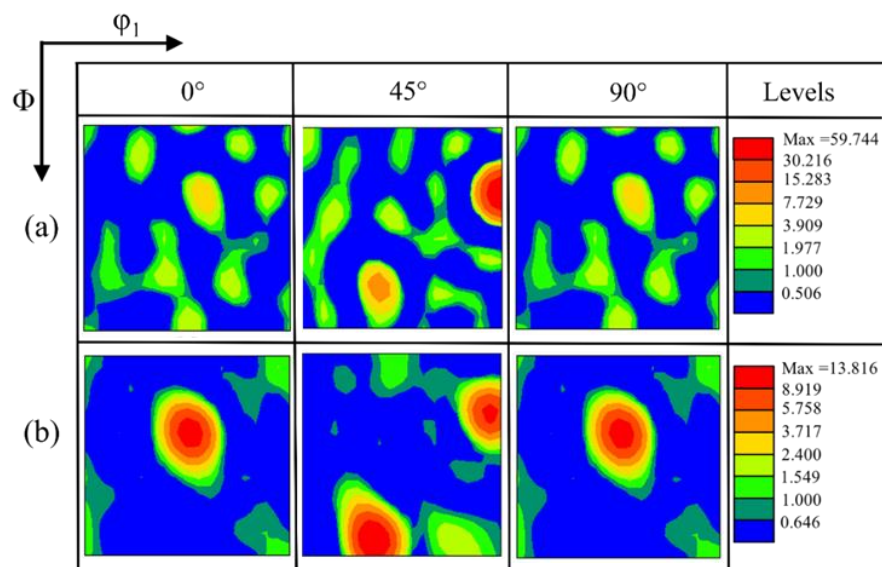
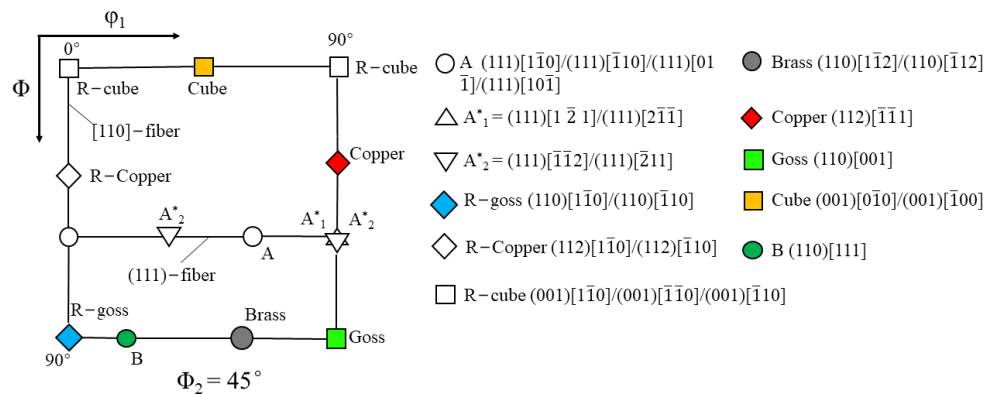
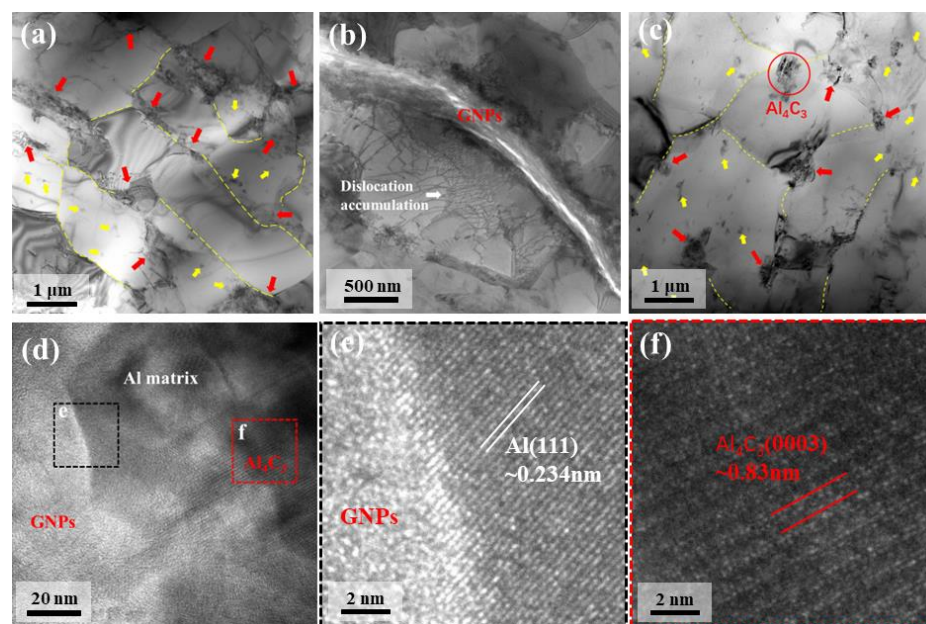


Figure 12. Orientation distribution function diagram of composite extruded by porthole die: (a) welding zone; (b) matrix zone.



**Figure 13.** The most ideal texture of aluminum and the corresponding Miller index on the ODF section when  $\phi_2 = 45^\circ$  [30].



**Figure 14.** TEM images of GNP/Al composites: (a–c) distribution of graphene; (d,e) HRTEM images of composites showing the interface between GNP and Al; (f)  $Al_4C_3$  in matrix.

### 3.5. Mechanical Properties

#### 3.5.1. Tensile Properties

Figure 15 presents representative tensile stress–strain curves for the composite and pure aluminum, and Figure 16 shows corresponding tensile properties. After the porthole die extrusion, the tensile strengths of the pure aluminum and the composite were 129.7 MPa and 139.7 MPa, respectively, and the elongations were 32.9% and 27.1%, respectively, in the extrusion direction (indicated as “0° direction”). Perpendicular to the extrusion direction (indicated as “90° direction”), the tensile strengths of the pure aluminum and composite were 118.5 MPa and 126.3 MPa, respectively, and the elongations were 15.6% and 24.1%, respectively. It should be noted that the tensile properties were lower in the 90° direction than in the 0° direction and that not all the samples in the 90° direction fractured close to the weld zone. This indicates that the tensile properties of the weld zone are higher than the measured values, and proves that the welding quality of graphene–aluminum matrix composites is reliable. It is especially noteworthy that, in the 90° direction, the elongation of the composite was 54.63% higher than that of the pure aluminum, indicating that GNP can not only strengthen the weld zone but also improve the transverse toughness of the longitudinal weld.

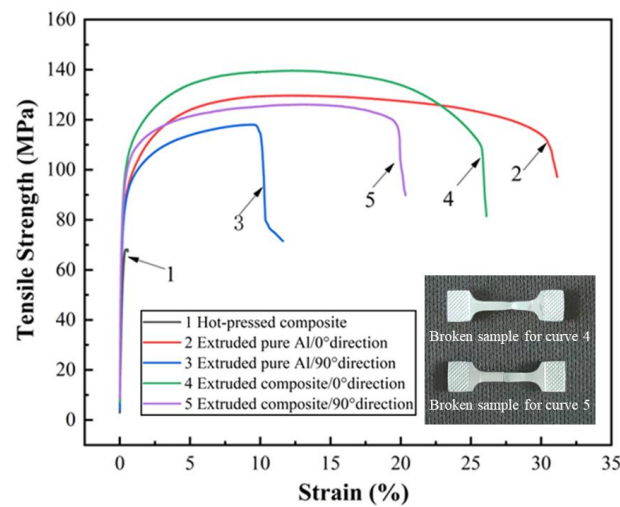


**Figure 15.** Representative tensile stress–strain curves of composites hot-pressed and extruded by the porthole die.

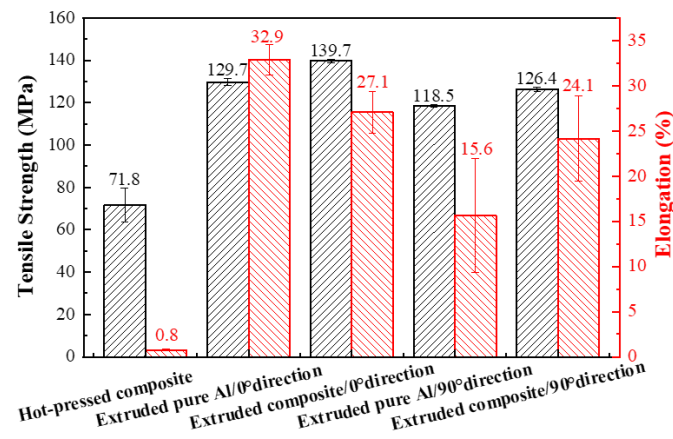


**Figure 16.** Tensile properties for composites and pure aluminum.

### 3.5.2. Microhardness

Vickers hardness tester (model Q10M) was used in the hardness test with a load force of 10 g, and a holding time of 10~15 s. Figure 17 shows microhardness distribution along a lengthwise direction on cross-sections of pure aluminum and composite extrudates. It can be seen that the hardness of the composite is higher than that of the pure aluminum; in addition, for both the pure aluminum and the composite, the hardness values are almost symmetrically distributed on both sides of the weld line. Hardness is lowest in the weld zone and rises with increased distance from this zone. From the matrix zone to the weld zone, hardness decreases considerably, due to the increase in the average grain size [31].

### 3.6. Fractography

Figure 18 shows fractography images of hot-pressed and porthole-die-extruded composites, among them, Figure 18c,f,i is EDS carbon element analysis. In Figure 18a,b, it can be seen that, due to the low temperature in the hot pressing process, the metallurgical properties of this composite are not good. The fracture surface presents the characteristics of a typical intergranular layered fracture (there are almost no obvious dimples), and this explains the very low elongation of the hot-pressed composite. At the same time, the GNP can be observed on multiple layers. The interface between the GNP and the aluminum matrix is weak and is unable to effectively carry the load transfer when subjected to the tensile force. Figure 18d,e show the fractography of the porthole-die-extruded composites in the 0° direction. In these images, it can be seen that the dimples are relatively uniform

and deep (obvious ductile fracture characteristics), the tear edges are bright, and there is no obvious free graphene in the dimples, indicating that the graphene and the aluminum matrix are well bonded so that graphene can fulfill its reinforcement role. This fractography also serves to explain the high tensile properties recorded in Figures 15 and 16. Figure 18g,h show the tensile fractography of the porthole-die-extruded composite in the 90° direction. In these images, it can be seen that, compared with the 0° direction, there are more large, shallow, and flat dimples, with less uniform distribution, and ductile fracture characteristics which are not as obvious as those in the 0° direction. This is mainly the result of anisotropy caused by the inevitable grain orientation of the extrudates [36].

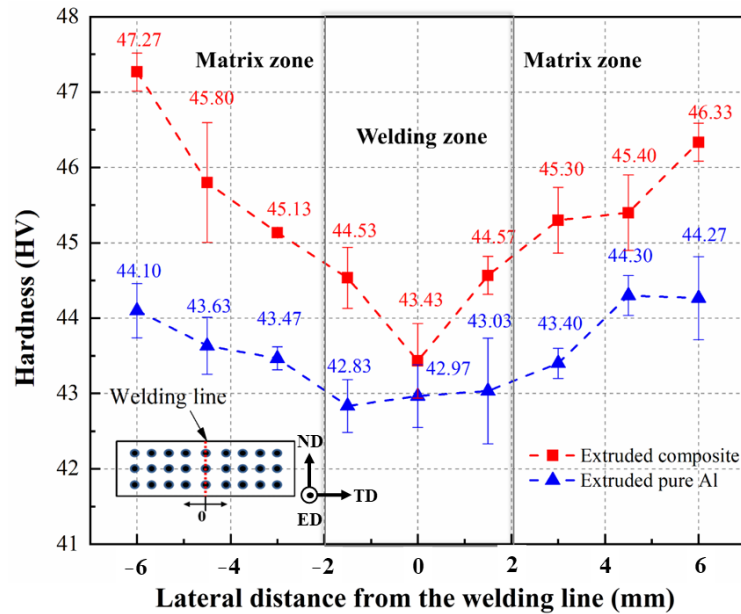


Figure 17. Microhardness on cross-sections of extruded composite and pure aluminum.

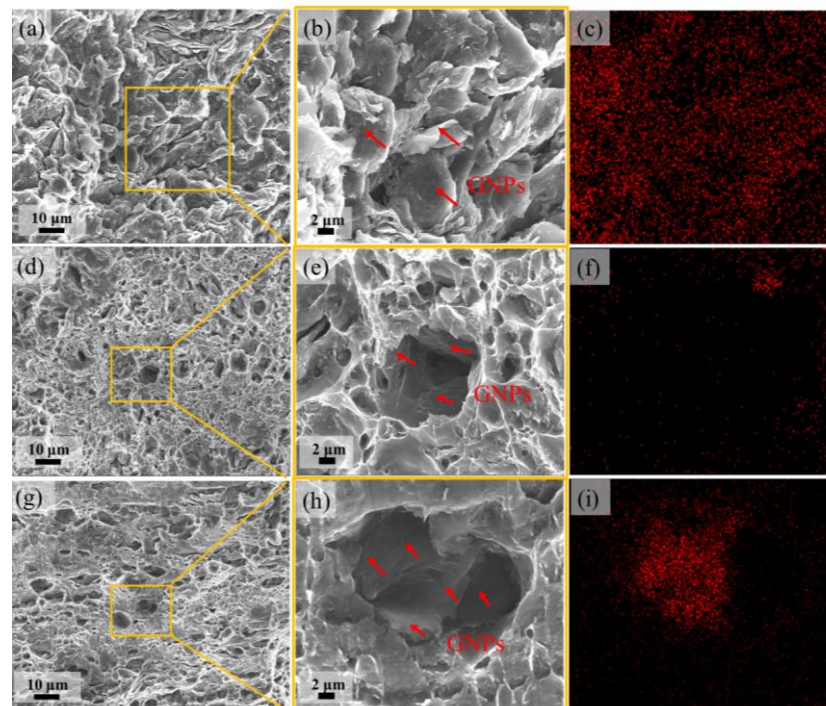


Figure 18. SEM fractography of the composite: (a–c) hot-pressed; (d–f) extruded/0° direction; (g–i) extruded/90° direction. (The red arrow points to GNPs).

#### 4. Conclusions

In this study, a 0.5 wt.% GNP/Al composite was extruded by a porthole die. The microstructure, morphology, and mechanical properties in the weld zone were then analyzed. Observations regarding metallographic morphology and tensile fracture morphology revealed an inexistence of micro-holes in the welding zone. However, obvious plastic deformation was observed at the tensile fracture, indicating that this was not a dangerous brittle fracture and that the extruded product had a certain damage tolerance. EBSD and TEM microscopic characterization revealed that dynamic recrystallization occurred during the porthole die extrusion process, and fine grains were generated, which helped to improve the mechanical properties of the profile. TEM characterization analysis of different positions on the welding surface during the extrusion process confirmed that the 0.5 wt.% GNP/Al composite exhibited reliable weld performance. Further conclusions can be stated as follows:

(1) The texture type in the weld zone of the extruded composite was copper texture (112) [111], and its intensity was relatively high. In the matrix zone, the texture types were copper texture (112) [111] and texture (110) [111], both at relatively low levels of intensity.

(2) Micro-level GNP was uniformly dispersed at the grain boundary, and nano-level GNP inside the grain was observed along the extrusion direction in the weld zone of the composites. This inhibited dislocation movement and improved the fracture strength of the material. Close bonding of GNP and the matrix was also observed in images obtained under high resolution. Finally, we found that some Al<sub>4</sub>C<sub>3</sub> was pinned at the grain boundary, inhibiting boundary migration and improving interfacial bonding strength further.

(3) In the extrusion direction, the tensile strength of the porthole-die-extruded composite reached 139.66 MPa, and elongation reached 27.06%; in the transverse direction, maximum values of 126.37 MPa tensile strength and 24.14% elongation were recorded, which were higher than the values obtained for pure aluminum by 6.65% and 54.63%, respectively. These results indicated that GNP promotes the strength and toughness of the porthole-die-extruded composite; Microhardness values were almost symmetrically distributed on both sides of the weld zone; however, microhardness in the welding zone was lower than in the matrix.

(4) Fractographic images of the sample in the extrusion direction revealed obvious ductile fracture characteristics: relatively deep and uniform dimples and bright tear edges, indicating a perfect interface between the GNP and the matrix that enabled the enhancement role of the GNP to be fulfilled. In the transverse direction, the characteristics of ductile fracture were not so obvious: large and flat dimples, which were shallower than those in the extrusion direction, mainly because of the grain orientation of the extruded material.

**Author Contributions:** S.L. and Q.W. conceived the concepts and ideas. P.C. and L.R. prepared the experimental samples, and X.B. collected and analyzed the experimental data. Y.L., B.C. and S.L. discussed the data and wrote the manuscript. All authors have read and agreed to the published version of the manuscript.

**Funding:** This research was supported by the Key project of the Shandong Provincial Natural Science Foundation, China (ZR2020KE013), National Natural Science Foundation of China (No. 51705295), University Qing Chuang science and technology plan of Shandong (No. 2019KJB015) and SDUST Research Fund (No. 2018TDJH101).

**Data Availability Statement:** The data supporting the findings of this study are available from the corresponding author.

**Conflicts of Interest:** The authors declare no conflict of interest.

## References

1. Awad, M.; Hassan, N.M.; Kannan, S. Mechanical properties of melt infiltration and powder metallurgy fabricated aluminum metal matrix composite. *Proc. Inst. Mech. Eng. Part B* **2021**, *235*, 2093–2107. [[CrossRef](#)]
2. Ali, R.; Ali, F.; Zahoor, A.; Shahid, R.N.; He, T.; Shahzad, M.; Asghar, Z.; Shah, A.; Mahmood, A.; Awais, H.B. Effect of sintering path on the microstructural and mechanical behavior of aluminum matrix composite reinforced with pre-synthesized Al/Cu core-shell particles. *J. Alloys Compd.* **2021**, *889*, 161531. [[CrossRef](#)]
3. Rathore, S.; Singh, R.K.R.; Khan, K.L.A. Effect of Process Parameters on Mechanical Properties of Aluminum Composite Foam Developed by Friction Stir processing. *Proc. Inst. Mech. Eng. Part B J. Eng. Manuf.* **2021**, *235*, 1892–1903. [[CrossRef](#)]
4. Mao, Y.; Li, J.; Vivek, A.; Daehn, G.S. High strength impact welding of 7075 Al to a SiC-reinforced aluminum metal matrix composite. *Mater. Lett.* **2021**, *303*, 130549. [[CrossRef](#)]
5. Turan, M.E.; Rashad, M.; Zengin, H.; Topcu, I.; Sun, Y.; Asif, M. Effect of Multiwalled Carbon Nanotubes on Elevated Temperature Tensile and Wear Behavior of Al2024 Matrix Composites Fabricated by Stir Casting and Hot Extrusion. *J. Mater. Eng. Perform.* **2020**, *29*, 5227–5237. [[CrossRef](#)]
6. Yi, L.-F.; Yoshida, N.; Onda, T.; Chen, Z.-C. Effect of Processing Conditions on Microstructure and Thermal Conductivity of Hot-Extruded Aluminum/Graphite Composites. *Mater. Trans.* **2019**, *60*, 136–143. [[CrossRef](#)]
7. Ogawa, F.; Yamamoto, S.; Masuda, C. Strong, ductile, and thermally conductive carbon nanotube-reinforced aluminum matrix composites fabricated by ball-milling and hot extrusion of powders encapsulated in aluminum containers. *Mater. Sci. Eng. A* **2018**, *711*, 460–469. [[CrossRef](#)]
8. Khademian, M.; Alizadeh, A.; Abdollahi, A. Fabrication and Characterization of Hot Rolled and Hot Extruded Boron Carbide (B<sub>4</sub>C) Reinforced A356 Aluminum Alloy Matrix Composites Produced by Stir Casting Method. *Trans. Indian Inst. Met.* **2017**, *70*, 1635–1646. [[CrossRef](#)]
9. Dong, C.-G.; Cui, R.; Wang, R.-C.; Peng, C.-Q.; Cai, Z.-Y. Microstructures and mechanical properties of Al 2519 matrix composites reinforced with Ti-coated SiC particles. *Trans. Nonferrous Met. Soc. China* **2020**, *30*, 863–871. [[CrossRef](#)]
10. Singh, A.P.; Yang, F.; Torrens, R.; Gabbitas, B. The effect of heat treatment on the mechanical properties of Ti-6Al-4V alloy produced by consolidating a high impurity blended powder mixture using a combination of powder compact hot pressing and extrusion. *J. Mater. Res.* **2019**, *34*, 1426–1438. [[CrossRef](#)]
11. Xu, Z.G.; Jiang, L.T.; Zhang, Q.; Qiao, J.; Wu, G.H. The microstructure and influence of hot extrusion on tensile properties of (Gd+B<sub>4</sub>C)/Al composite. *J. Alloys Compd.* **2017**, *729*, 1234–1243. [[CrossRef](#)]
12. Alizadeh, A.; Abdollahi, A.; Radfar, M.J. Processing, characterization, room temperature mechanical properties and fracture behavior of hot extruded multi-scale B<sub>4</sub>C reinforced 5083 aluminum alloy based composites. *Trans. Nonferrous Met. Soc. China* **2017**, *27*, 1233–1247. [[CrossRef](#)]
13. Li, T.; Wang, Y.; Yang, M.; Hou, H.; Wu, S. High strength and conductivity copper/graphene composites prepared by severe plastic deformation of graphene coated copper powder. *Mater. Sci. Eng. A* **2021**, *826*, 141983. [[CrossRef](#)]
14. Li, W.; Liu, Y.; Wu, G. Preparation of graphite flakes/Al with preferred orientation and high thermal conductivity by squeeze casting. *Carbon* **2015**, *95*, 545–551. [[CrossRef](#)]
15. Lou, S.; Wang, A.; Lu, S.; Guo, G.; Qu, C.; Su, C. Tensile property and micro-texture evolution of the charge weld in a billet-to-billet extrusion of AA6061 aluminum profile. *Int. J. Adv. Manuf. Technol.* **2019**, *103*, 1309–1323. [[CrossRef](#)]
16. Yu, J.; Zhao, G.; Chen, L. Analysis of longitudinal weld seam defects and investigation of solid-state bonding criteria in porthole die extrusion process of aluminum alloy profiles. *J. Mater. Process. Technol.* **2016**, *237*, 31–47. [[CrossRef](#)]
17. Xu, X.; Zhao, G.; Wang, Y.; Chen, X.; Zhang, C. Microstructural evolution and its effect on mechanical properties of spray deposited 2195 alloy during porthole die extrusion process. *Vacuum* **2019**, *167*, 28–39. [[CrossRef](#)]
18. Bai, S.-W.; Fang, G.; Zhou, J. Analysis of the bonding strength and microstructure of AA6082 extrusion weld seams formed during physical simulation. *J. Mater. Process. Technol.* **2017**, *250*, 109–120. [[CrossRef](#)]
19. Yu, J.; Zhao, G.; Cui, W.; Zhang, C.; Chen, L. Microstructural evolution and mechanical properties of welding seams in aluminum alloy profiles extruded by a porthole die under different billet heating temperatures and extrusion speeds. *J. Mater. Process. Technol.* **2017**, *247*, 214–222. [[CrossRef](#)]
20. Chen, G.; Chen, L.; Zhao, G.; Lu, B. Investigation on longitudinal weld seams during porthole die extrusion process of high strength 7075 aluminum alloy. *Int. J. Adv. Manuf. Technol.* **2017**, *91*, 1897–1907. [[CrossRef](#)]
21. Fan, X.; Chen, L.; Chen, G.; Zhao, G.; Zhang, C. Joining of 1060/6063 aluminum alloys based on porthole die extrusion process. *J. Mater. Process. Technol.* **2017**, *250*, 65–72. [[CrossRef](#)]
22. Yu, J.; Zhao, G.; Zhao, X.; Chen, L.; Chen, M. Microstructures of longitudinal/transverse welds and back-end defects and their influences on the corrosion resistance and mechanical properties of aluminum alloy extrusion profiles. *J. Mater. Process. Technol.* **2019**, *267*, 1–16. [[CrossRef](#)]
23. Lou, S.M.; Qu, C.D.; Guo, G.X.; Ran, L.W.; Liu, Y.Q.; Zhang, P.P.; Su, C.J.; Wang, Q.B. Effect of Fabrication Parameters on the Performance of 0.5 wt.% Graphene Nanoplatelets-Reinforced Aluminum Composites. *Materials* **2020**, *13*, 3483. [[CrossRef](#)] [[PubMed](#)]
24. Gao, X.; Yue, H.; Guo, E.; Zhang, H.; Lin, X.; Yao, L.; Wang, B. Preparation and tensile properties of homogeneously dispersed graphene reinforced aluminum matrix composites. *Mater. Des.* **2016**, *94*, 54–60. [[CrossRef](#)]

25. Xiang, S.L. Microstructure and Mechanical Properties of Graphene Nanosheets Reinforced Magnesium Matrix Composites. Ph.D. Thesis, Harbin Institute of Technology, Harbin, China, 2018. [[CrossRef](#)]
26. Dresselhaus, M.S.; Jorio, A.; Hofmann, M.; Dresselhaus, G.; Saito, R. Perspectives on Carbon Nanotubes and Graphene Raman Spectroscopy. *Nano Lett.* **2010**, *10*, 751–758. [[CrossRef](#)] [[PubMed](#)]
27. Lou, S.; Liu, Y.; Qu, C.; Guo, G.; Ran, L.; Zhang, P.; Su, C. Influence of a Hot Extrusion with Rectangular-Section on Mechanical Properties and Microstructure of 0.5wt% Graphene Nanoplatelet-Reinforced Aluminum Composites. *Adv. Eng. Mater.* **2021**, *23*, 2001127. [[CrossRef](#)]
28. Sharma, A.; Sharma, V.M.; Mewar, S.; Pal, S.K.; Paul, J. Friction stir processing of Al6061-SiC-graphite hybrid surface composites. *Mater. Manuf. Process.* **2018**, *33*, 795–804. [[CrossRef](#)]
29. Berbenni, S.; Favier, V.; Berveiller, M. Impact of the grain size distribution on the yield stress of heterogeneous materials. *Int. J. Plast.* **2006**, *23*, 114–142. [[CrossRef](#)]
30. Li, C.J.; Sun, H.F.; Li, X.W.; Zhang, J.L.; Fang, W.B.; Tan, Z.Y. Microstructure, texture and mechanical properties of Mg-3.0Zn-0.2Ca alloys fabricated by extrusion at various temperatures. *J. Alloys Compd.* **2015**, *652*, 122–131. [[CrossRef](#)]
31. Xu, X. Investigation on Solid-State Welding Behavior, Microstructure and Properties of Longitudinal Weld in Al-Li Alloy Porthole Die Extrusion Profiles. Ph.D. Thesis, Shandong University, Jinan, China, 2021. [[CrossRef](#)]
32. Fan, X.; Tang, D.; Fang, W.; Li, D.; Peng, Y. Microstructure development and texture evolution of aluminum multi-port extrusion tube during the porthole die extrusion. *Mater. Charact.* **2016**, *118*, 468–480. [[CrossRef](#)]
33. Knieke, C.; Berger, A.; Voigt, M.; Taylor, R.N.K. Scalable production of graphene sheets by mechanical delamination. *Carbon* **2010**, *48*, 3196–3204. [[CrossRef](#)]
34. Sharma, A.; Morisada, Y.; Fujii, H. Bending induced mechanical exfoliation of graphene interlayers in a through thickness Al-GNP functionally graded composite fabricated via novel single-step FSP approach. *Carbon* **2022**, *186*, 475–491. [[CrossRef](#)]
35. Yu, Y.H.; Yang, W.S.; Zhou, C.; Zhang, N.B.; Chao, Z.L. Effect of ball milling time on graphene nanosheets reinforced Al6063 composite fabricated by pressure infiltration method—ScienceDirect. *Carbon* **2019**, *141*, 25–39. [[CrossRef](#)]
36. Zhang, F.; Su, X.; Chen, Z.; Nie, Z. Effect of welding parameters on microstructure and mechanical properties of friction stir welded joints of a super high strength Al–Zn–Mg–Cu aluminum alloy. *Mater. Des.* **2015**, *67*, 483–491. [[CrossRef](#)]

**Disclaimer/Publisher’s Note:** The statements, opinions and data contained in all publications are solely those of the individual author(s) and contributor(s) and not of MDPI and/or the editor(s). MDPI and/or the editor(s) disclaim responsibility for any injury to people or property resulting from any ideas, methods, instructions or products referred to in the content.